CHAPTER IV
RESULTS AND DISCUSSION

4.1 Characterization of Precursors

4.1.1 Silatrane

Silatrane was synthesized by the Oxide One Pot Synthesis (OOPS) process. The product obtained was a white powder and the structure was shown in Figure 4.1. Thermal properties of the synthesized material analyzed by TGA show in Figure 4.2, giving one major transition of the weight loss at 400°C with 18.13 % ash yield, corresponding to $Si((OCH_2CH_2)_3N)_2H_2$. The % ash yield was close to the theoretical ceramic yield (18.63%) of the corresponding product. Moreover, FTIR spectrum (Figure 4.3) showed the characteristic peak of silatrane at 785 to 729 and 579 cm^{-1} corresponding to Si-O-C and Si←--N, respectively (Charoenpinitkarn *et al.*, 2001).

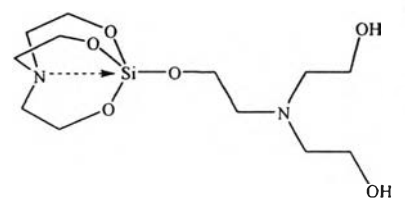

Figure 4.1 The structure of silatrane precursor.

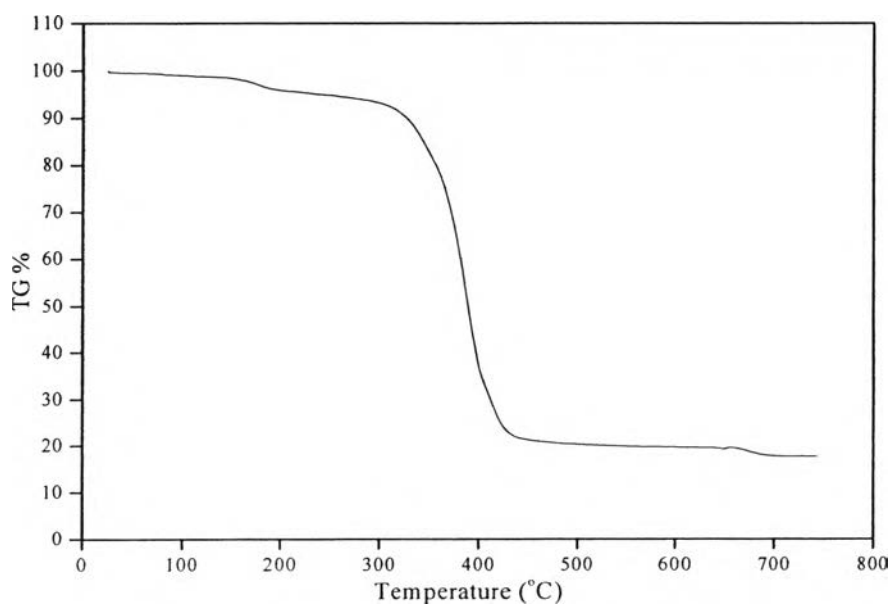

Figure 4.2 TGA result of silatrane precursor.

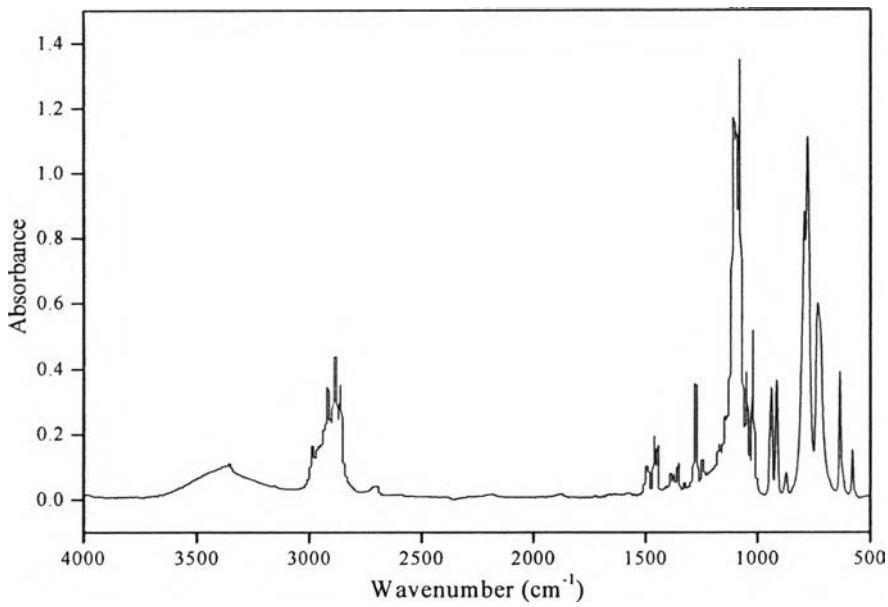

Figure 4.3. FTIR spectrum of silatrane precursor.

4.1.2 Molybdenum glycolate

The molybdenum glycolate was synthesized by the OOPS process to obtain white solid and the structure is shown in Figure 4.4. TGA result shows five mass loss transitions: 150°C (H_2O molecule absorbed by molybdenum glycolate molecule), 210°C (H_2O molecule generated from decomposition of molybdenum glycolate), 300° and 430°C (glycolate ligand of molybdenum glycolate molecule), and 720°C (carbon residues) with 52.5% ash yield, as shown in Figure 4.5, corresponding to $Mo(OH)_2(O(CH_2)_2O)_2$ having 56.7% theoretical ceramic yield. The FTIR result (Figure 4.6) shows the bands at 946 and 533 cm^{-1}, assigning to the Mo-O-C and Mo-O stretching, respectively. (Sutara *et al.*, 2004)

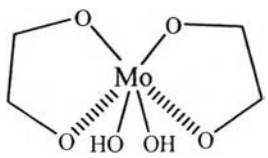

Figure 4.4 The structure of molybdenum glycolate.

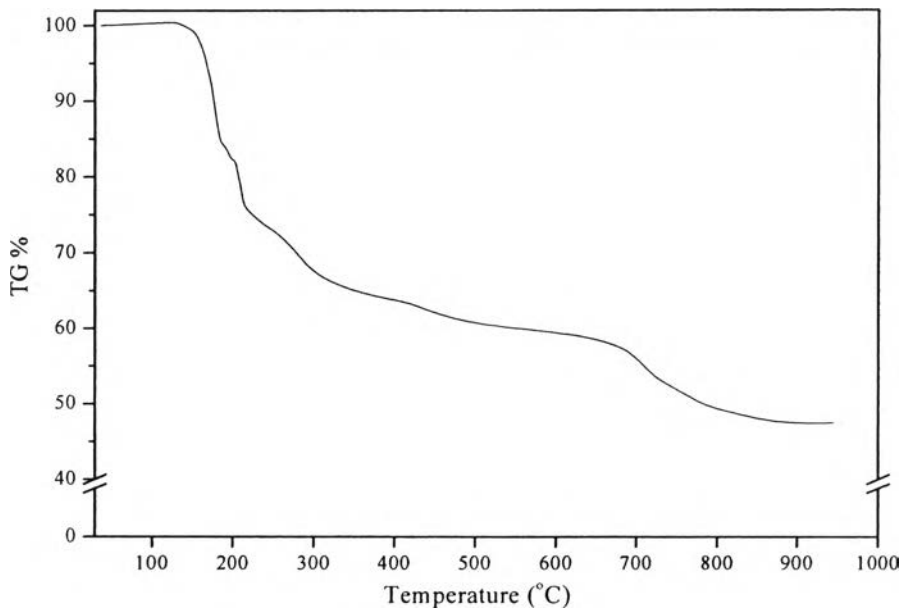

Figure 4.5 TGA thermogram of molybdenum glycolate.

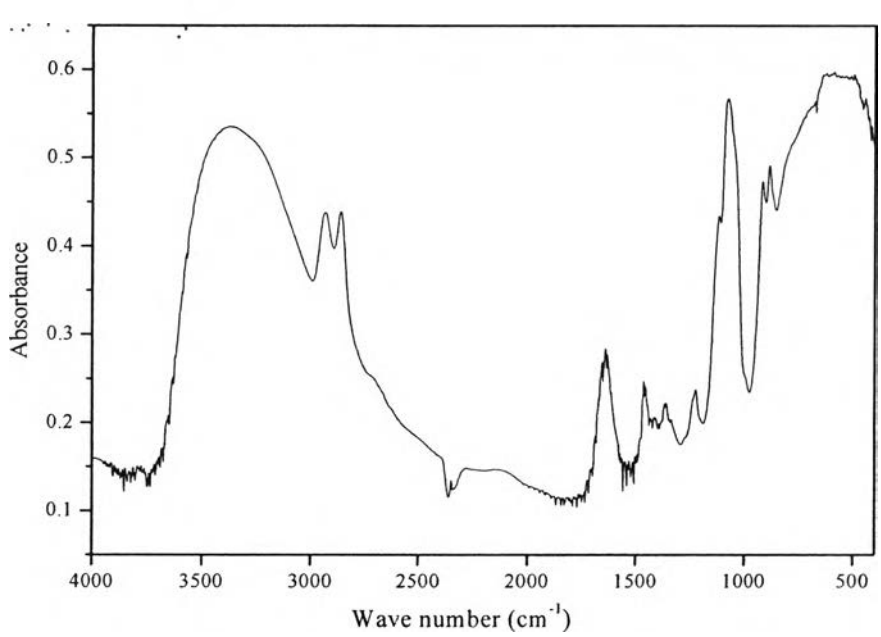

Figure 4.6 FTIR result for molybdenum glycolate.

4.2 Characterization of Mo-SBA-1 Catalysts

Mo-SBA-1 was synthesized via the sol-gel process to obtain white powder. The XRD patterns of calcined Mo-SBA-1 products are shown in Figure 4.7. All the samples showed three well resolved XRD diffraction peaks at 2θ of 2.2°, 2.4° and

2.6°, which are indexed to the {200}, {210}, and {211} reflections, respectively. These diffraction peaks are the characteristics of the cubic *Pm3n* space group (Che *et al.*, 2002) and are the same manner as pure silica SBA-1 (Hou *et al.*, 1994). In addition, some weak peaks in the range of 3.5° to 6° indicate that the calcined sample has a high order cubic mesostructure, as described by Che *et al.* in 2001. However, the decrease of intensity of the {200} and {211} reflections with increasing molybdenum content in silica framework, suggests that the structure of Mo-SBA-1 with higher molybdenum content is less order than that with the lower one. Since the Mo-O bond length is longer than Si-O, the decrease in the {210} reflection of Mo-SBA-1, comparing to that of its pure SBA-1, could confirm the incorporation of molybdenum into SBA-1 framework (Ji *et al.*, 2005).

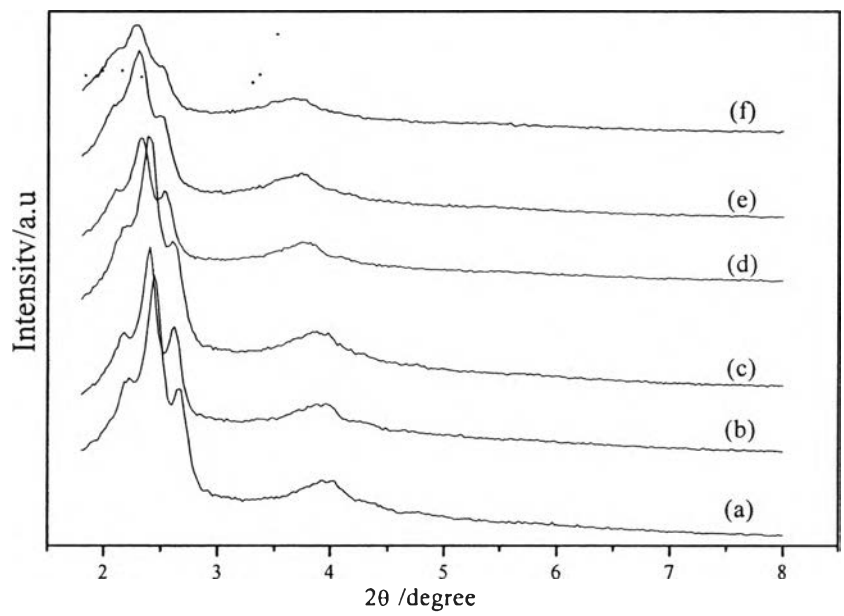

Figure 4.7 XRD patterns of the calcined SBA-1 samples containing: (a) 0.70, (b) 1.43, (c) 3.5, (d) 5.00, (e) 7.20, and (f) 10.0% Mo.

Diffuse reflectance UV-vis (DR-UV) spectrometer is used to determine local molecular coordination sphere and bonding information for inorganic compounds. The results are shown in Figure 4.8. According to Cotton *et al.* in 1980, ligand-metal charge transfer of oxomolybdenum compounds (O^{2-}–Mo^{6+}) caused the

adsorption band in the UV-visible region, and the position of this electronic transition depends on the ligand field symmetry surrounding the Mo center. The tetrahedral $Mo^{6+}(T_d)$ is expected to show a higher energy transition than the octahedral one (Weber *et al.*, 1995). The band at 230 nm is the characteristic peak of MoO^{4-} species due to the transition of an oxygen $2p\pi$ electron into empty d-orbital of molybdenum, as also found in Jeziorowski and coworkers' work in 1979. In addition, the 230 nm band also the indication of the MoO^{4-} species incorporated in the silica framework via Mo–O–Si bridge (Che *et al.*, 2001). The band at 250 nm corresponds to Mo^{6+} (T_d). Characteristic of MoO_3, octahedral Mo^{6+} species (O_h (t_{2u},t_{1g}→t_{2g})), is indicated by the band at 320 nm (Che. *et al.*, 2001). Therefore, the disappearance of the peak at 320 nm suggested the lack of MoO_3 ($Mo^{6+}(O_h)$). It is likely that most of Mo were incorporated in the silica SBA-1 framework (Che *et al.*, 2001) and had tetrahedral coordination as indicated by the band at 250 nm. From Figure 4.6, it is also found that 5% molybdenum can be introduced into SBA-1 framework without any extra-framework.

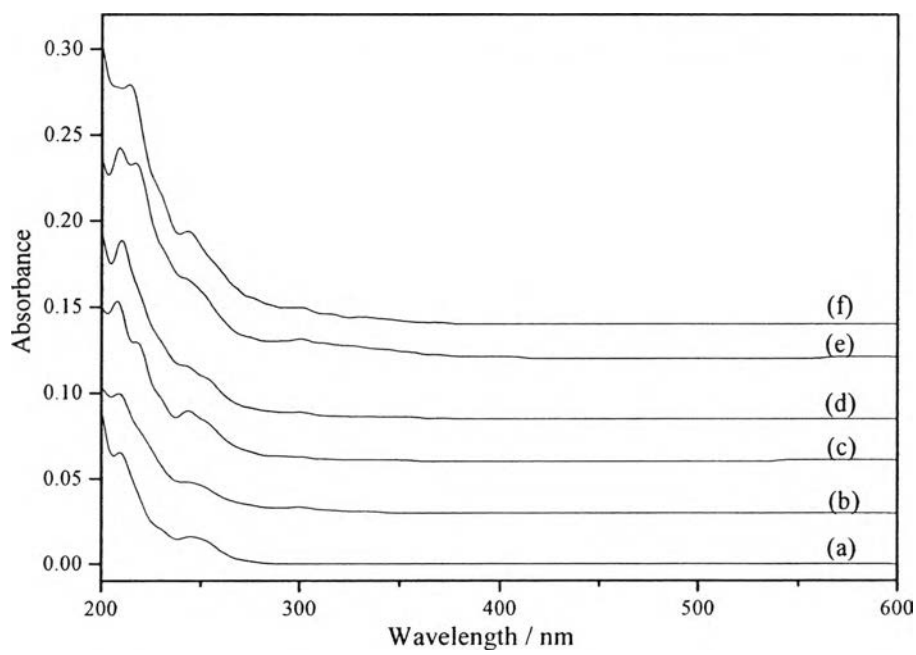

Figure 4.8 DRUV spectra of the calcined SBA-1samples containing: (a) 0.70, (b) 1.43, (c) 3.5, (d) 5.00, (e) 7.20, and (f) 10.0% Mo.

The functional group of the synthesized Mo-SBA-1 samples was investigated using FTIR shown in Figure 4.9. Generally, the broad band at about 3500 cm^{-1} and the peak at around 1640 cm^{-1} are the O–H stretching of Si–OH and the bending of physisorbed water. The strong peaks at 1080 and 800 cm^{-1} are the asymmetric and symmetric stretching of Si–O–Si, directly related to the silica framework (Pavia *et al.*, 1996). The band at 456 cm^{-1} is corresponded to Si–O bending (Li *et al.*, 2003). Furthermore, a band at 968 cm^{-1} also indicates the asymmetric stretching of Si–O–Si of SBA-1, which is shifted to 963 cm^{-1} for the Mo-SBA-1 samples. The peak intensity was increased with the amount of molybdenum content. According to Morey *et al.* (2000), this asymmetric stretching of Si–O–Si could be shifted to a lower position when one silica atom is replaced with a heavier atom, implying that the molybdenum species were incorporated into silica framework.

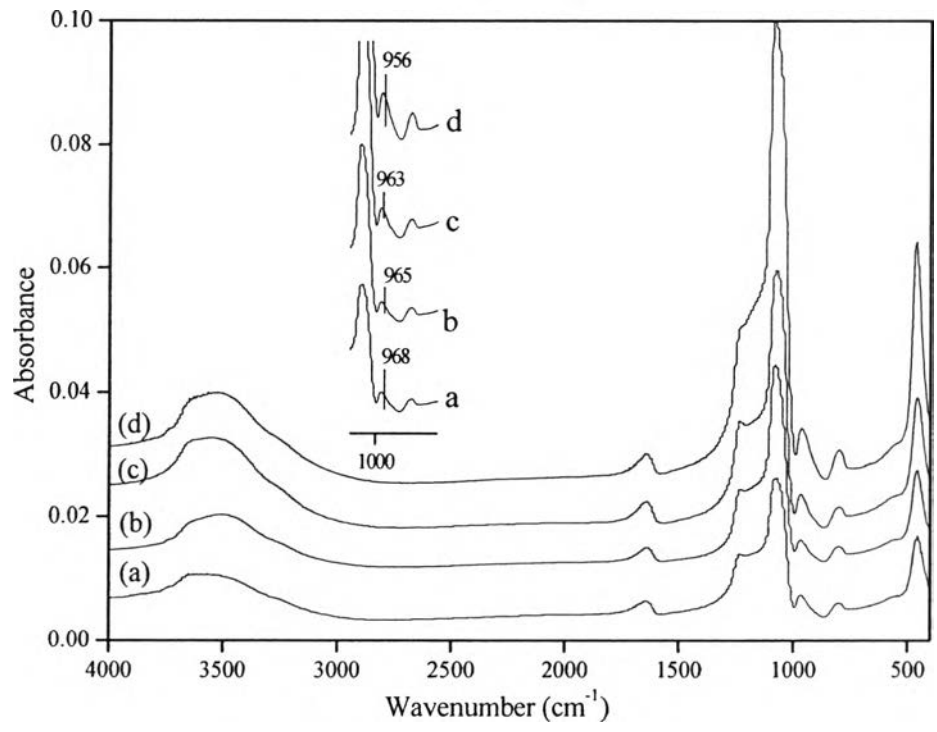

Figure 4.9 FTIR spectra of the synthesized Mo-BBA-1 materials: (a) pure SBA-1, (b) 0.07, (c) 1.43, and (d) 5.00 %Mo.

The scanning electron micrograph of the synthesized pure SBA-1 is shown in Figures 4.10. The clear crystal like external morphology of a octadecahedron (18 hedron) with 6 square {100} and 12 hexagon {110} planes is consistent with cubic structure observed by Guan *et al.* in 2000, and Lin *et al.* in 2002. When molybdenum species were incorporated into silica framework of SBA-1, the octadecahedron surface became more isotropic morphology, as shown in Figure 4.11. According to the surfactant-silica assembly mechanism proposed by Hou *et al.* in 1994, the formation of cubic *Pm3n* mesophase occurs through $S^+X^-I^+$ pathway under acidic condition and the final product is depended on the components of the reaction system. The difference in the surface morphology of pure SBA-1 and Mo-SBA-1 was considered in the difference of their inorganic (I^+) species concentration. In addition, the higher amount of the molybdenum results in the more difficulty of cubic *Pm3n* formation and more isotropic morphology was observed.

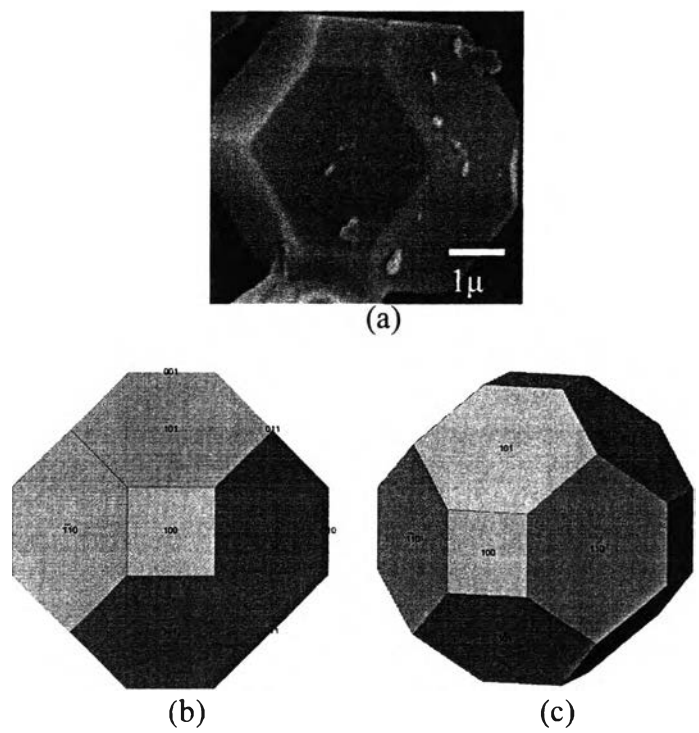

Figure 4.10 a) SEM image of the synthesized SBA-1, b) and c) the models of the SBA-1 particle with the plane index.

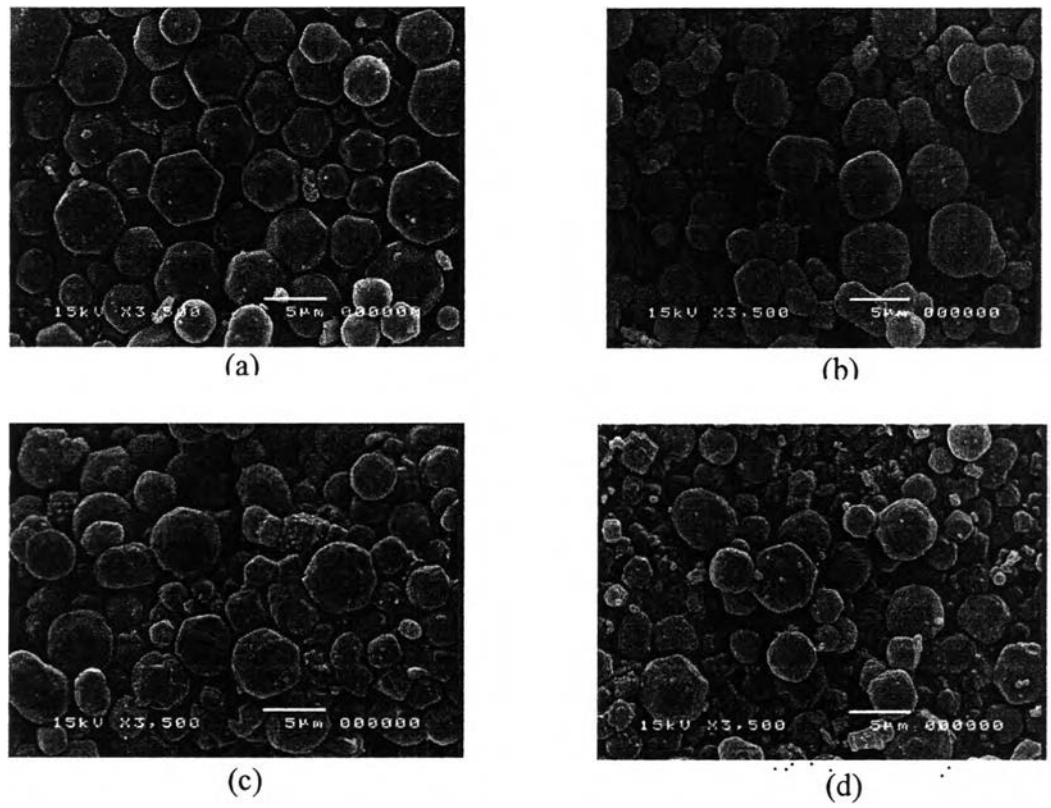

Figure 4.11 SEM images of the calcined SBA-1 samples containing: (a) 1.43, (b) 3.50, (c) 5.00, and (d) 7.20% Mo.

N_2 adsorption/desorption isotherms and their corresponding pore size distribution curves obtained from the desorption branch of the calcined Mo-SBA-1 samples containing various contents of Mo are presented in Figure 4.12. All samples exhibit isotherms of type IV adsorption isotherms, which is the typical characteristic of mesoporous solids (Inagaki *et al.*, 1996). The sharp inflection at a relative pressure of p/p_0 = 0.1-0.3 corresponds to capillary condensation within the uniform mesopores. The Mo-SBA-1 showed a very narrow pore size distribution with a pore diameter of about 21 Å, indicating that the structure of these materials was uniform (Figure 4.13). In addition, all samples showed the high surface area (>1000 m^2/g). The incorporation of molybdenum into the SBA-1 has significant effect on the specific surface area of the materials. With increasing molybdenum content, the specific surface area and pore volume decreased, as summarized in table 4.1. This can be explained by the destruction of the silica mesostructure with introducing molybdenum species, as also confirmed by the XRD result.

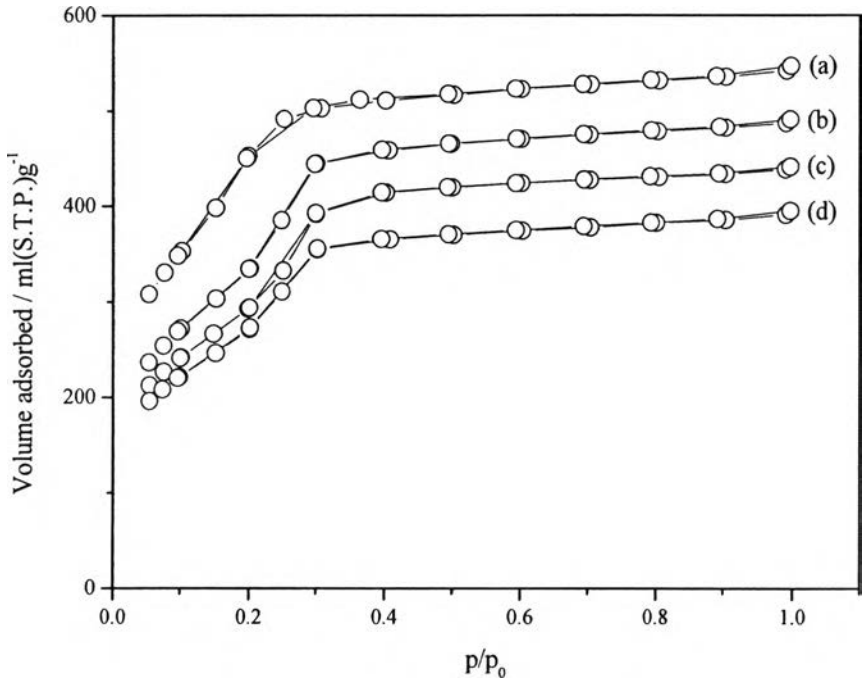

Figure 4.12 Nitrogen adsorption/desorption isotherms of the calcined SBA-1 samples containing (a) 1.43, (b) 3.50, (c) 5.00, and (d) 7.20% Mo.

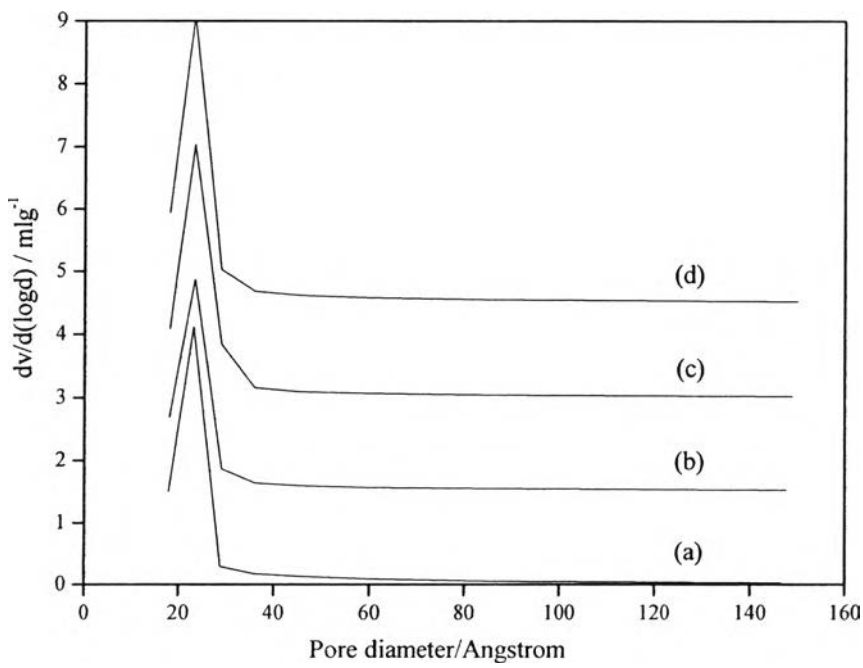

Figure 4.13 Pore size distributions of the calcined SBA-1 samples containing (a) 1.43, (b) 3.50, (c) 5.00, and (d) 7.20% Mo.

Table 4.1 Average pore diameters, pore volumes and surface areas of the calcined Mo-SBA-1 samples.

Sample	% Mo loaded	Average pore diameter (Å)	Pore volume (cm^3/g)	Surface area (m^2/g)
1	0	29.0	0.95	1520
2	2.40	21.35	0.69	1285
3	3.50	22.23	0.68	1219
4	5.30	22.63	0.67	1183
5	7.20	21.72	0.60	1114

4.3 Activity study of the synthesized Mo-SBA-1 catalyst

Catalysis activity of the synthesized catalysts was tested via epoxidation reaction of styrene monomer. This reaction was carried out in a batch type reactor using H_2O_2 as oxidant. After the reaction was finished and the catalyst was filtered, products obtained were analyzed by gas chromatography.

As shown in Figure 4.14, products of the reaction are only styrene oxide and benzaldehyde. The latter is the major product. Styrene conversion over pure SBA-1 was relatively low when comparing to Mo-SBA-1. The conversion of styrene monomer was strongly depended on the amount of molybdenum loaded. It increased as increasing the molybdenum content from 7.76±1.25 to 63.32±3.07% when the molybdenum content was loaded from 0 to 10%. This indicates that the molybdenum species in the SBA-1 framework was the activated site for the oxidation reaction. It is also revealed that the styrene conversion when using 0.70%Mo in SBA-1 is relatively high as compared to Ti-SBA-1 sample containing 0.86 %Ti, giving only 10.2 % styrene conversion (Ji *et al.*, 2005). However, the styrene oxide selectivity was relatively low compared to Ti-SBA-1 sample. The styrene oxide selectivity was also depended on the amount of the molybdenum content. It reached the highest value, 36.90±2.47%, at 7.20% molybdenum, but decreased to 14.49±3.34% when the molybdenum content was increased to 10.0%. This result could be explained by the lost of the well order pattern in the XRD results. For comparison, molybdenum impregnated onto SBA-1 framework was prepared and its catalytic activity was also

studied. The impregnated sample containing 7.0%Mo showed 14.74±1.54% conversion with 9.26±2.87% styrene oxide selectivity. This value is relatively low, as compared to the Mo-SBA-1 containing 7.20%Mo and synthesized via the sol-gel process. Higher dispersion and isolation of molybdenum sites incorporated into SBA-1 via the sol-gel process could be attributed for the enhancement of the catalytic performance in epoxidation reaction of styrene. This is also consistent with Rana *et al.* (1998) who reported that Mo-MCM-41 synthesized by hydrothermal technique showed higher activity for the oxidation of cyclohexane and gave higher stable cyclohexanol product, in comparison to the impregnated catalyst, due to the presence of tetrahedral coordination molybdenum on silica framework, resulting in the site of the active metal species.

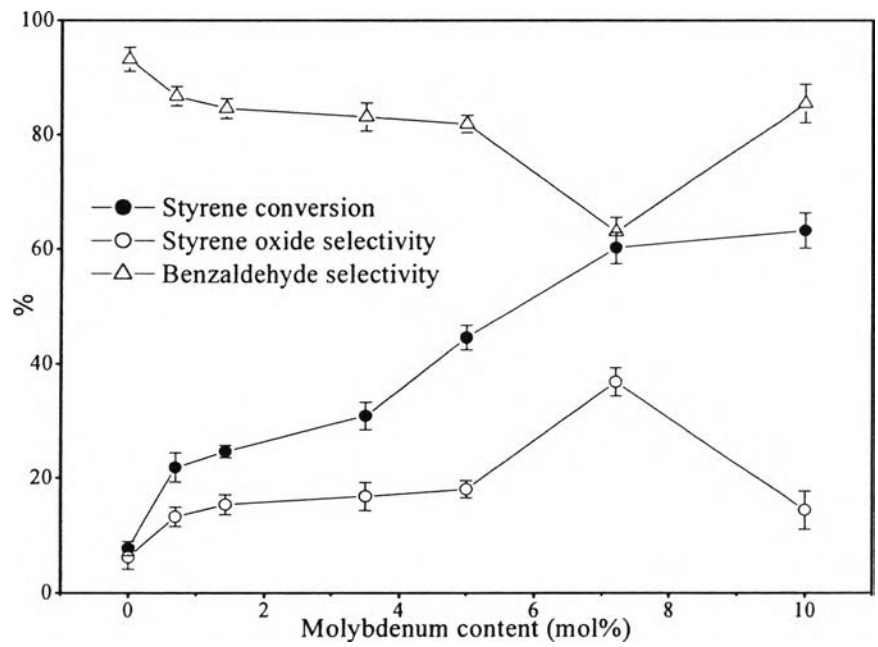

Figure 4.14 Effect of the molybdenum content on epoxidation of styrene carried out at 70°C reaction temperature for 3 h with 0.1g catalyst.

The effect of the reaction temperature was also investigated at three different temperatures in the range of 60° to 80°C; see Figure 4.15, showing the increase in the styrene conversion from 42.11±2.56 to 60.26±2.72% as increasing the reaction temperature from 60° to 70°C. Further increase of the reaction temperature to 80°C caused a decrease in styrene conversion to 46.04±3.12% due to the

decomposition of H_2O_2 at high temperature (Rode *et al.*, 2003). Similar trend was observed with styrene oxide selectivity, the highest styrene oxide selectivity, 36.90±2.47%, was observed when the reaction temperature was at 70°C, and decreased to 20.08±2.07% at 80°C while the selectivity of benzaldehyde was increased. It could be explained by the further oxidation of styrene oxide to benzaldehyde at higher temperature (Ji *et al.*, 2005).

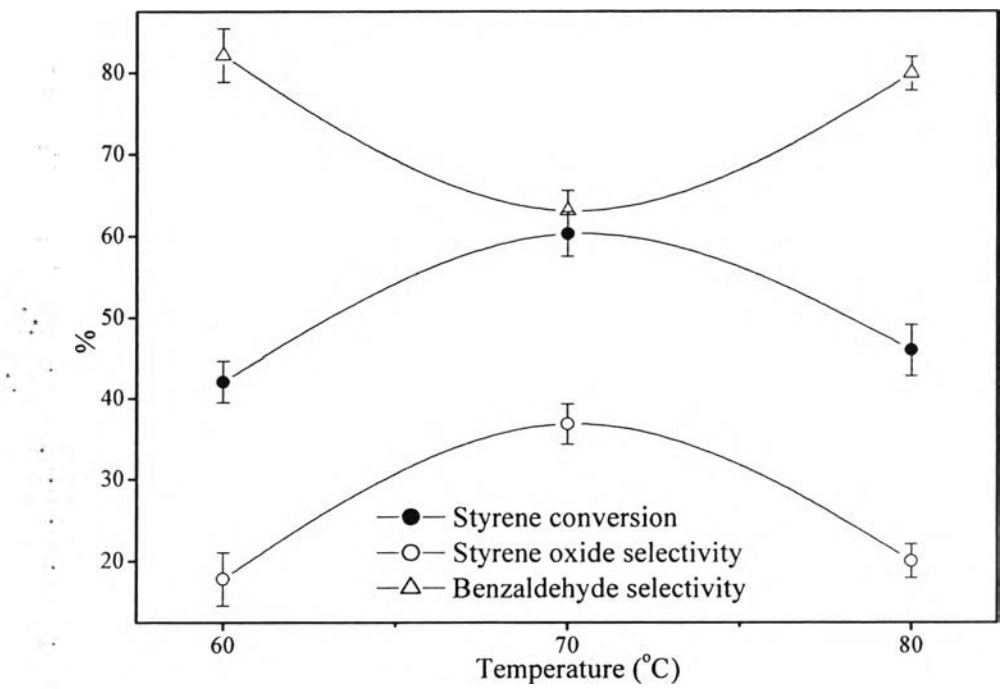

Figure 4.15 Effect of the reaction temperature on epoxidation of styrene using 0.1 g catalyst for 3 h reaction time.

Figure 4.16 illustrate the reaction time effect at 70°C reaction temperature. Expectedly, the styrene conversion increased with the reaction time. The reaction was fast at the beginning owing to the full amount of H_2O_2 oxidant (Ji *et al.*, 2005). The maximum styrene oxide selectivity, 26.33±1.94%, was reached at 3 h reaction time and slightly decreased with a corresponding increase in benzaldehyde selectivity. This result is consistent with the work of Ji *et al.* (2005) who reported that the formation of benzaldehyde could be attributed to the secondary oxidation of epoxide.

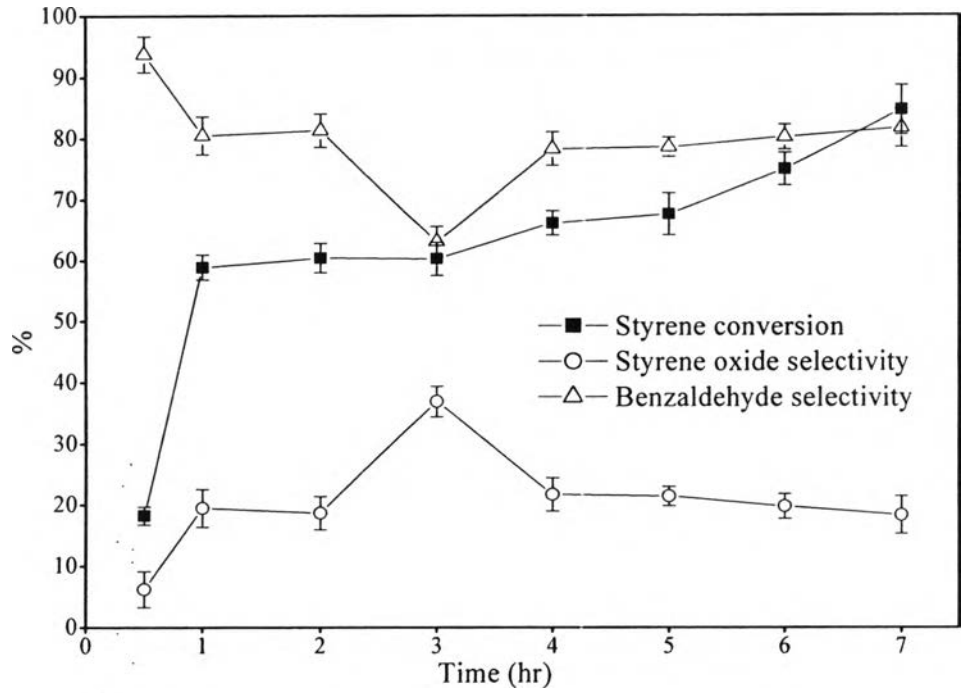

Figure 4.16 Effect of the reaction time on the epoxidation of styrene using 0.1 g catalyst at 70°C reaction temperature.

The last factor studied was the amount of the catalyst used, as summarized in Figure 4.17. Styrene conversion reached 60.26±2.72% when catalyst used was 0.10 g and did not significantly change, comparing with 0.20 and 0.30 g of catalyst. The maximum styrene oxide selectivity was observed at 0.1 g catalyst used. Therefore, optimum catalyst used was 0.1 g.

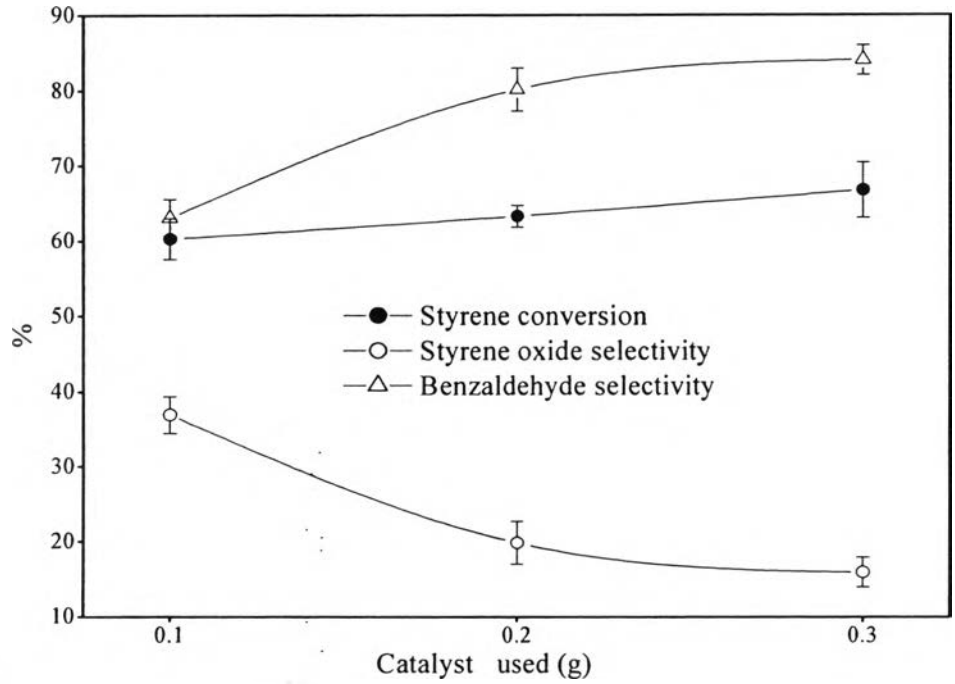

Figure 4.17 Effect of the catalyst used on the epoxidation of styrene at 70°C reaction temperature for 3 h reaction time.